Cement & Concrete Composites 38 (2013) 40–49

Contents lists available at SciVerse ScienceDirect

Cement & Concrete Composites

journal homepage: www.elsevier.com/locate/cemconcomp

Properties of binary and ternary reactive MgO mortar blends subjected to CO_2 curing

Daman K. Panesar [a], Liwu Mo [a,b,*]

[a] Department of Civil Engineering, University of Toronto, Toronto, Ontario, Canada M5S 1A4
[b] College of Materials Science and Engineering, Nanjing University of Technology, No. 5 Xinmofan Road, Nanjing, Jiangsu 210009, China

ARTICLE INFO

Article history:
Received 10 October 2012
Received in revised form 25 January 2013
Accepted 20 March 2013
Available online 28 March 2013

Keywords:
Microstructure
Carbonation
Acceleration
MgO
Compressive strength

ABSTRACT

Research and development of low CO_2 binders for building material applications is warranted in efforts to reduce the negative environmental impacts associated with the cement and concrete industry. The purpose of this study is to investigate the effect of carbonation curing on the mineralogy, morphology, microstructure and evolution of compressive strength of mortars comprised of general use (GU) cement, ground granulated blast furnace slag (GGBFS), and reactive MgO used as cement replacement. This study investigates binary (GU–MgO) and ternary (GU–GGBFS–MgO) blends exposed to atmosphere curing (0.0038%CO_2) and carbonation curing (99.9%CO_2). Carbonation-cured mortars exhibited greater compressive strengths than atmosphere mortars at all ages (7 d, 28 d, and 56 d). Increasing percentages of reactive MgO decreased the compressive strength markedly less for carbonation-cured mortars than atmosphere-cured mortars particularly due to magnesium calcite formations. Magnesium calcite influenced the morphology of carbonates and promoted the carbonate agglomeration resulting in a dense and interconnected microstructure.

1. Introduction

Concrete is one of the most widely used construction materials in the world. However, the current process for manufacturing cement, the main binder component of concrete, is extremely energy intensive and contributes to 5% of global anthropogenic CO_2 emissions [1]. For decades, waste materials such as fly ash (FA), ground granulated blast furnace slag (GGBFS) and silica fume have been used as supplementary cementing materials (SCMs) to replace conventional Portland cement, largely owing to their beneficial effect on concrete durability. van den Herde and de Belie [2] have shown that although the use of GGBFS and FA can be beneficial based on cost, little advantage is reported when considering environmental impacts particularly CO_2 and SO_x emissions and total energy used. The use of SCMs alone is not sufficient to reduce negative global impacts associated with the cement and concrete industry. Owing to increasing awareness of the impacts of CO_2 emissions on the global climate, the cement industry is seeking ways to reduce its CO_2 emissions, decrease raw material inputs and lower the energy intensiveness of its processes. However, it is not enough to simply use recycled waste material in the form of SCMs to replace relatively expensive conventional Portland cement.

The development of alternative low CO_2 binders such as calcium sulfoaluminate cement, alkali-activated binder, and reactive MgO cement to partially replace conventional Portland cement is gaining attention in the effort to reduce CO_2 levels and the energy demands associated with the cement industry [3–6]. Reactive MgO is typically manufactured by calcining magnesite at a low temperature (i.e., approximately 750 °C), which is much lower than the 1450 °C necessary to produce Portland cement clinker. However, unlike SCMs, reactive MgO as cement replacement does not exhibit obvious pozzolanic or latent hydraulic properties, but rather it requires CO_2 exposure to gain mechanical properties [7]. A feasible application for the use of reactive MgO cured at elevated CO_2 concentrations is precast elements such as masonry units that can be well-carbonated in a plant setting.

The carbonation of traditional concrete materials has been investigated primarily because of its potential detrimental effect on reinforcing steel corrosion. However, carbonation has also been reported to cause densification, reduce permeability, increase compressive strength and act as a CO_2 sink as a result of the formation of calcium carbonate ($CaCO_3$) [8,9]. In Portland cement systems, the formation of $CaCO_3$ during carbonation is briefly described by the following equation:

$$Ca^{2+}(aq) + CO_3^{2-}(aq) \rightarrow CaCO_3(s) \quad (1)$$

* Corresponding author at: College of Materials Science and Engineering, Nanjing University of Technology, No. 5 Xinmofan Road, Nanjing, Jiangsu 210009, China.
E-mail addresses: d.panesar@utoronto.ca (D.K. Panesar), andymoliwu@sohu.com (L. Mo).

0958-9465/$ - see front matter © 2013 Elsevier Ltd. All rights reserved.
http://dx.doi.org/10.1016/j.cemconcomp.2013.03.009

The Ca^{2+} is typically provided by dissolution and/or decalcification of portlandite ($Ca(OH)_2$), ettringite, calcium silicate hydrates (CSH), anhydrous C_2S, and anhydrous C_3S. If the cementing materials contain SCMs then the Ca^{2+} may also be present as a result of pozzolanic reactions. The amount of CO_3^{2-} is influenced by the concentration and pressure of CO_2 and is supplied by the dissolution of CO_2 into the pore solution after the CO_2 penetrates the material's microstructure. A relatively higher CO_2 concentration (i.e., 2–20%) than atmosphere CO_2 levels (0.038%) coupled with 60–70% relative humidity has been typically employed to accelerate the carbonation rate of concrete materials [10–12]. In addition, it should be noted that the amount and type of SCMs used in concrete materials influences the rate of carbonation [13]. As reported by Stark and Ludwig [14], in contrast to the GU cement concrete, the occurrence of carbonation reactions at the exposed surface of concrete containing GGBFS yields an increase in capillary porosity in particular, the volume of very large capillary pores (>100 nm), which has been attributed to the formation of soluble metastable calcium carbonates. This may be beneficial for the CO_2 ingress.

The carbonation rate of reactive MgO and its implications on the properties of hardened concrete is strongly influenced by the CO_2 concentration [7,15]. At atmospheric CO_2 concentrations (approximately 0.038%), no obvious benefit of compressive strength development was observed in masonry units containing reactive MgO as Portland cement replacement, due to the very slow rate of carbonation of reactive MgO [7,15]. In contrast, masonry units containing reactive MgO exposed to a 20% CO_2 concentration had a greater rate of compressive strength development compared to Portland cement masonry units [15,16]. This was attributed to the formation of magnesium carbonates such as nesquehonite ($MgCO_3{\cdot}3H_2O$), dypingite ($Mg_5(CO_3)_4(OH)_2{\cdot}5H_2O$) and artinite ($Mg_2(OH)_2CO_3{\cdot}3H_2O$) [15,16]. Vandeperre and Al-Tabbaa [17] found that cement paste containing reactive MgO carbonated faster when exposed to an environment with a 20% concentration of CO_2 and 98% relative humidity than specimens exposed to a 5% CO_2 concentration and 65% relative humidity. From a chemical thermodynamic perspective, various magnesium minerals can form in a $MgO–CO_2–H_2O$ reaction system [18,19]. However, the formation of magnesium carbonates is strongly kinetically controlled and is influenced by several factors such as temperature, CO_2 pressure and ionic strength [18,19].

Examining the response of cement-based materials exposed up to a 99% CO_2 concentration has attracted attention not only because of the beneficial effects on some material properties but also because of the potential for CO_2 sequestration [9,13,20,21]. In comparison with traditional steam curing, the CO_2 curing of concrete yields an increased rate of strength development due to the formation of $CaCO_3$ [9,20]. de Silva et al. [22] synthesized $CaCO_3$ carbonate binders by carbonating hydrated lime using industrial-grade CO_2. They found that the main factor controlling its compressive strength was the morphology of $CaCO_3$. Specifically, well-developed crystal carbonate resulted in a higher compressive strength. Another study by de Silva [23] exposed a blend consisting of $Ca(OH)_2$ and $Mg(OH)_2$, to an accelerated carbonation condition of 20 atm. pressure of CO_2. They reported that the carbonate binder consisted primarily of calcium- and magnesium-containing carbonates as well as a $MgCO_3{\cdot}3H_2O$ phase, which exhibited a higher strength than the calcium carbonate binder [23].

Although there is published literature on carbonation curing and some studies have been conducted on the use of reactive MgO in cement-based materials, there is a dearth of knowledge on the effect of carbonation that uses reactive MgO in ternary blends with GU and GGBFS on the mineralogical formations, morphology and evolution of compressive strength. A recent investigation on the reactive MgO–GU cement paste system exposed to a 99.9% CO_2 concentration reported significant findings regarding the formation of calcium- and magnesium-based carbonates and the evolution of microhardness and microstructure for reactive MgO cement pastes [24]. As an extension of that research, this study examines a more complex system of reactive MgO–GU–GGBFS mortar blends. Six mortar mix designs are examined which have up to 40% reactive MgO as cement replacement and up to 40% GGBFS as cement replacement. Two curing regimes, atmospheric curing and carbonation curing, which expose specimens to 0.038% and 99.9% CO_2 concentration, respectively, are investigated. This study examines the development of compressive strength, microstructure and morphology at days 7, 28 and 56 using analytical techniques, including scanning electron microscopy (SEM), X-ray diffraction (XRD), backscattered scanning electron microscopy (BSEM), and differential thermal analysis (DTA).

2. Experimental program

2.1. Materials, sample preparation and curing

2.1.1. Materials

General use (GU) Portland cement and GGBFS from Holcim Canada were used in this study. Reactive MgO was supplied by Liyang Special Materials Company, China. The reactive MgO was prepared by calcining magnesite at approximately 800 °C and consists mainly of magnesia (MgO) and a small amount of undecomposed magnesite. Table 1 presents the chemical composition of the GU, GGBFS and reactive MgO. The fine aggregate that was used was natural silica sand with a specific gravity, fineness modulus and absorption of 2.74%, 2.85% and 1.4%, respectively.

2.1.2. Sample preparation and curing

All six mortars have a water-to-binder (w/b) ratio of 0.52 and a weight ratio of cementitious binder to sand of 1.0:2.75. For each mixture, the proportions of the cementitious binder are shown in Table 2. The mortars designated as B-0, B-20 and B-40 are GU-based cements with 0%, 20% and 40% reactive MgO as cement replacement, respectively. The GU–GGBFS-based mortars designated as T-0, T-20 and T-40, and all contain 40% GGBFS as cement replacement and 0%, 20% and 40% reactive MgO as cement replacement, respectively.

For each mix, twenty-four 50 mm × 50 mm × 50 mm mortar cube specimens were cast in accordance with ASTM C109/C 109M-07 [25]. After casting the samples, they were immediately placed in a chamber with 98% relative humidity and a temperature of 23 ± 2 °C for 2 d, demoulded, and then placed back in the curing chamber for an additional 7 d. Each specimen was then exposed to the laboratory environment (60 ± 2% relative humidity, and a temperature of 23 ± 2 °C) for 3 d, and then placed into a desiccator with silica gel and vacuumed using a Leybold Trivac C D8A pump for 1 d to remove excessive water. The purpose of the pre-drying process was to facilitate the ingress of CO_2 [24,26]. Subsequently, at 13 d of age, the 24 specimens for each mixture were then separated into two sets of 12 cubes. One set of specimens was cured in sealed chambers with an atmospheric environment of approximately 0.038% CO_2 concentration, a temperature of 23 ± 2 °C, and a relative humidity of 98% until testing at days 7, 28, and 56. This set of specimens is representative of and referred to as "atmosphere-cured specimens".

The second set of specimens was placed in sealed chambers consisting of 99.9% CO_2 concentration, temperature of 23 ± 2 °C, and a relative humidity of 98% until tested at 7 d, 28 d, and 56 d of exposure. The CO_2 with a 99.9% concentration was first injected from a compressed CO_2 cylinder into a large (1000 l) plastic buffer bag that was connected to the sample chamber. Accordingly, the pressure of CO_2 in the buffer bag was equivalent to the atmo-

Table 1
Chemical compositions of GU cement, GGBFS and reactive MgO (% by mass).

	MgO	CaO	SiO_2	Al_2O_3	Fe_2O_3	Na_2O	K_2O	SO_3	LOI*
GU cement	2.34	60.94	19.24	5.43	2.36	0.22	1.11	4.11	3.06
GGBFS	11.36	37.94	37.24	8.70	0.35	0.43	0.43	2.68	0.83
MgO	89.67	1.65	0.36	0.23	0.34	0.23	0.06	–	7.15

* LOI: Loss on ignition.

Table 2
Mix proportions of cement used in mortars (wt.%).

Mix identity	GU–MgO blends			GU–MgO–GGBFS blends		
	B-0	B-20	B-40	T-0	T-20	T-40
GU cement	100	80	60	60	40	20
Reactive MgO	0	20	40	0	20	40
GGBFS	0	0	0	40	40	40

spheric pressure. Prior to the injection of CO_2 into the sample chamber, the sealed chamber was vacuumed to remove the air. The valve was then opened and CO_2 from the buffer bag was injected into the chamber until the gas pressure in the chamber was equal to that in the buffer bag. As a result of CO_2 consumption due to carbonation processes, additional CO_2 was continually supplied into the chamber by the buffer bag. The buffer bag was refilled with CO_2 from the cylinder before complete consumption of the CO_2 in the buffer bag. The relative humidity in the chamber was controlled using a supersaturated K_2SO_4 solution. This set of specimens is referred to as "carbonation-cured specimens".

2.2. Test procedures

2.2.1. Carbonation front

After exposure to the 99.9% CO_2 environment (accelerated carbonation condition), the carbonation front of the carbonation-cured specimens was tested by spraying a 1% phenolphthalein solution on the fresh split surface.

2.2.2. Compressive strength

The compressive strength of specimens was tested after 7 d, 28 d and 56 d of exposure to the atmosphere-curing chamber or the 99.9% CO_2-curing chamber. For each test, the averages of three compressive strength values were measured and the corresponding coefficient of variation of the mortar mixtures was calculated.

2.2.3. Carbonate phases identification

Powder samples were prepared by gently grinding the mortar specimens with a mortar and pestle. During the grinding process, as much sand as possible was removed by passing the powder through a 0.5 mm sieve. The passed powders were then ground to a particle size of less than 75 μm. The crystalline phases in the powder samples were investigated using XRD with Cu Kα radiation (λ = 1.5418 Å), 2θ range of 5–80°, and a step size of 0.02°. The powder samples were also investigated by DTA using a NETZSCH STA 409. A temperature range of 25–1050 °C at a heating rate of 10 °C/min with a nitrogen gas flow of 50 ml/min was used.

2.2.4. Microstructure characterization

A JEOL JSM6610-Lv SEM coupled with an Oxford Energy-Dispersive X-ray (EDX) spectroscopy was used for the microstructural and chemical analysis of the specimens. Fractured mortar samples were gold sputter coated and examined with SEM to investigate the morphology. In addition, a small sample of approximately 15 mm × 15 mm × 15 mm cut from the central mortar specimen was embedded into epoxy resin, polished, carbon coated, and then investigated using BSEM.

3. Results and discussion

3.1. Carbonation front

Fig. 1 shows freshly split surfaces that were exposed to the carbonation-curing regime for 56 d and then sprayed with a phenolphthalein solution. The B-0 specimen shows an obvious red[1] color throughout the surface, which indicates a large amount of uncarbonated $Ca(OH)_2$. Increasing the percentage of reactive MgO decreases the red area on the surface, which indicates an increase in carbonation degree. However, the carbonation front of the partially carbonated B-0, B-20 and B-40 samples is unclear. Chang and Chen [27] revealed that the partly carbonated zone with a carbonation degree of 0–50% and pH values between 9.0 and 11.5, could not be identified with phenolphthalein because the boundary pH of the phenolphthalein indicator is generally 9.0, which corresponds to 50% carbonation degree.

By 56 d, the T-0 mortar specimen shows a clear carbonation front with the depth of the fully carbonated zone being approximately 4 mm. Although the T-0, T-20 and T-40 specimens were not fully carbonated, the uncarbonated (red zone) area clearly decreases as the amount of reactive MgO increases. The greater carbonation front observed for the T-0, T-20 and T-40 specimens, when compared to the B-0, B-20 and B-40 specimens, may be due to the relatively coarser pore structure of the former, which facilitates CO_2 ingress due to the presence of 40% GGBFS as cement replacement. The results from Fig. 1 show that increasing the percentage of reactive MgO increases the carbonation degree. This is particularly apparent for B-40 and T-40, which shows that the CO_2 has almost penetrated through the specimens.

3.2. Compressive strength

Table 3 shows the average compressive strength of specimens exposed to atmosphere curing and carbonation curing. The average values are based on three measurements. In all cases, the coefficient of variation is between 1.7% and 6.3%. In general, the compressive strength of all specimens increases with an increase in the curing age, irrespective of the curing regime or the presence of reactive MgO.

At 7 d, the atmosphere-cured T-0 mortar exhibits slightly lower compressive strengths compared to B-0, and by 28 d, the mean compressive strength of T-0 was slightly (2 MPa) greater than that of the B-0 mortar. The lower 7 d strength of T-0 is expected due to the latent hydraulic and pozzolanic reactions of GGBFS as cement replacement. Mixtures containing 20% and 40% reactive MgO combined with 40% GGBFS, namely, T-20 and T-40 had mean compressive strengths between 1 to 4.6 MPa less than that of B-20 and B-40, respectively. The results in Table 3 also show that increasing the amount of reactive MgO used as cement replacement signifi-

[1] For interpretation of color in Fig. 1, the reader is referred to the web version of this article.

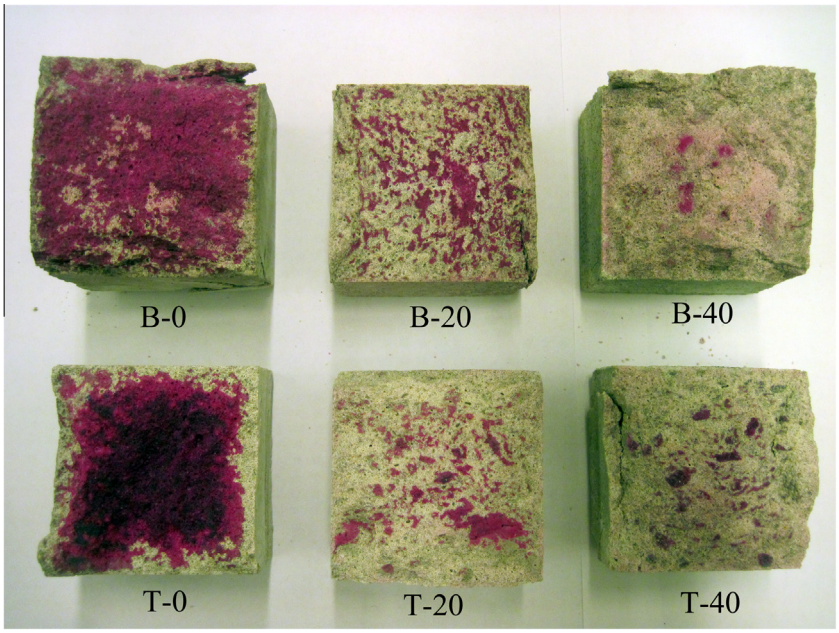

Fig. 1. Split fresh surfaces of cement mortar specimens sprayed with a phenolphthalein solution after 56 d of carbonation curing.

Table 3
Compressive strength of mortar cubes containing 0–40% reactive MgO after atmosphere curing and carbonation curing (MPa).

	Exposure time (d)	B-0	B-20	B-40	T-0	T-20	T-40
Atmosphere curing	7	31.7	18.8	11.9	30.0	15.7	10.3
	28	34.4	21.9	12.7	37.7	17.3	13.2
	56	37.7	23.7	15.5	39.8	21.1	14.5
Carbonation curing	7	35.2	21.5	24.9	35.9	18.7	20.9
	28	45.3	42.5	40.5	45.4	33.5	31.6
	56	47.1	45.9	47.7	48.1	41.6	34.9

cantly decreased the compressive strength for all mixtures exposed to atmosphere curing. This is believed to be due to the larger quantity of GU cement replaced by reactive MgO and GGBFS, which reduces the cement hydration products and results in lower compressive strength. This is due to a lower fraction of hydraulic and or latently hydraulic material, and a relatively higher fraction of reactive MgO which does not contribute to strength gain until and unless it undergoes carbonation processes. Compared to the atmosphere-cured specimens, the carbonation cured specimens had higher compressive strengths for the same mix design at the same age. Closer examination of the carbonation cured measurements shows that the B-0 and T-0 specimens exhibited similar strength gain from day 7 to 56. This suggests that the response of GGBFS mortars exposed to 99.9% CO_2 concentration and 98% relative humidity is a departure from the literature which reports the behavior of concrete or mortars containing GGBFS exposed to typical laboratory accelerated carbonation conditions (i.e. CO_2 concentrations of up to 20% and 40–80% relative humidity). At 56 d, the compressive strengths of carbonation-cured mortars B-0, B-20, B-40, T-0, T-20 and T-40 were 1.2, 1.9, 3.1, 1.2, 2.0 and 2.4 times higher than that of the corresponding atmosphere-cured specimens, respectively. This is expected to be associated with the formation of carbonate phases during the carbonation-curing process and will be discussed further in Section 3.3.

For the carbonation-cured specimens, the compressive strength increased as the curing duration also increased. It was also observed that the rate of compressive strength development was greater from 7 d to 28 d, compared to the rate of strength development from 28 d to 56 d. The compressive strength of T-40 after 56 d of carbonation was 34.9 MPa, which is close to 37.7 MPa of compressive strength in the atmosphere-cured B-0 specimen at the same age.

3.3. Carbonate phases formed in the mortars

Fig. 2 shows the XRD patterns of powders from the atmosphere-cured and carbonation-cured mortars after 56 d of curing. Fig. 2a presents the XRD patterns for mixtures containing GU and reactive MgO as cement replacement, and Fig. 2b presents the XRD patterns for mortars containing 40% GGBFS as cement replacement and up to 40% reactive MgO.

For carbonation-cured B-0, B-20 and B-40 specimens, clear diffraction peaks of calcite ($CaCO_3$) are apparent in Fig. 2a. In all cases, diffraction peaks for $Ca(OH)_2$, ettringite were present even after 56 d of curing. In addition, the atmosphere-cured B-0 mortar showed unhydrated calcium silicates. Weak peaks of unhydrated magnesia and undecomposed magnesite are also apparent in the atmosphere cured B-40 mortars. With increasing percentages of reactive MgO used as cement replacement, the intensities of $Ca(OH)_2$ and ettringite peaks weaken. This may be related to the greater degree of carbonation and less GU cement used in the specimens containing larger amounts of reactive MgO. For the B-20 and B-40 specimens, magnesium calcite was formed due to the presence of Mg in $CaCO_3$, though it was challenging to distinguish between the calcite and magnesium calcite due to their overlapping peaks [23]. Nevertheless, the formation of magnesium calcite was

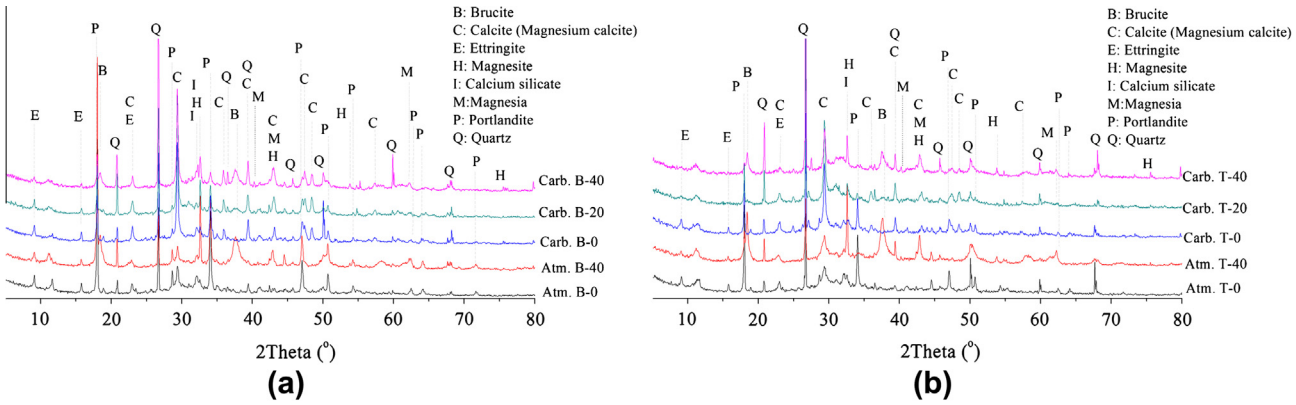

Fig. 2. XRD patterns of powder samples from atmosphere-cured and carbonation-cured specimens after 56 d of exposure: (a) GU-reactive MgO blends and (b) GU-GGBFS-reactive MgO blends.

confirmed by the EDX results discussed in Section 3.4. Besides the hydration products of GU cement, clear diffraction patterns of brucite ($Mg(OH)_2$) are apparent in the atmosphere-cured B-40 specimen, which is due to the hydration of reactive MgO.

Fig. 2b presents the XRD pattern for atmosphere cured and carbonation cured specimens containing 40% GGBFS and from 0% to 40% reactive MgO. For the T-0, and T-40 specimens exposed to atmosphere curing, $Ca(OH)_2$, ettringite, unhydrated calcium silicate were the main crystalline phases as shown in Fig. 2b. For the T-40 specimen, brucite ($Mg(OH)_2$) was also observed in the atmosphere cured specimens and was confirmed in Section 3.4 based on the SEM analysis. The results in Fig. 2b also show that $CaCO_3$ was formed in the carbonation-cured T-0 specimen while magnesium calcite was formed in carbonation-cured T-20 and T-40 specimens.

Fig. 3 shows the typical DTA curves of powder samples from the atmosphere-cured and carbonation-cured specimens after 56 d of exposure. After B-40 was atmosphere-cured, three clear endothermic peaks appear at 100–320 °C, 320–460 °C, and 460–540 °C, which correspond to the dehydration of calcium silicate hydrate (C–S–H), $Mg(OH)_2$ and $Ca(OH)_2$, respectively. In comparison with the atmosphere-cured B-40 sample, three key differences were observed in the carbonated samples. Firstly, the carbonation-cured B-0 specimen shows a markedly smaller endothermic peak of $Ca(OH)_2$ compared to the atmosphere-cured B-40 sample indicating that $Ca(OH)_2$ was partially consumed due to carbonation processes. The carbonated B-40 and T-40 specimens have very weak dehydration peak of $Ca(OH)_2$ compared to the carbonated B-0 sample which may be attributed to less $Ca(OH)_2$ due to less GU cement and a relatively higher carbonation of $Ca(OH)_2$.

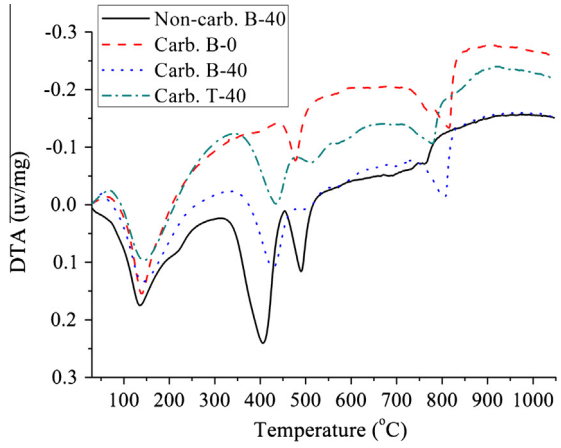

Fig. 3. Typical DTA curves of powder samples from atmosphere-cured and carbonation-cured mortar specimens after 56 d of exposure.

Secondly, in all the carbonation-cured specimens, an endothermic peak at a range of 720–900 °C due to the decarbonation of well-crystallized $CaCO_3$ was observed. It should be noted, however, that some poorly crystallized $CaCO_3$ may also exist and will usually decarbonate at lower temperatures (i.e., 540–720 °C) [21].

Thirdly, in carbonation-cured B-40 and T-40 specimens, the endothermic peak of $Mg(OH)_2$ (at 320–460 °C) is much smaller compared to that of the atmosphere-cured B-40 specimen, indicating some carbonation of the $Mg(OH)_2$ phases.

3.4. SEM morphology

Fig. 4a and b shows SEM images of the B-0 mortar after 56 d of atmosphere curing and carbonation curing, respectively. Fig. 4a shows a considerable amount of amorphous CSH and the formation of large bulk $Ca(OH)_2$ crystals in the atmosphere-cured specimen. CSH and $Ca(OH)_2$ also exist in the carbonation-cured samples shown in Fig. 4b. These results are also supported by the phenolphthalein test and the XRD results shown in Figs. 1 and 2a. Although $CaCO_3$ was formed in the carbonation-cured B-0 specimen, according to XRD analysis in Fig. 2a, it is difficult to clearly distinguish this in Fig. 4b, probably due to the small crystal size of $CaCO_3$.

In contrast to the B-0 specimen, the microstructure of 56 d carbonation-cured specimens containing reactive MgO was markedly different from that of the atmosphere-cured mortars. For the atmosphere-cured B-40 specimen, Fig. 5a illustrates an abundance of platy $Mg(OH)_2$ crystals due to the hydration of reactive MgO. The $Mg(OH)_2$ crystals coexist with cement hydration products and cover the surfaces of other phases in the specimen. The microstructure of the B-40 specimen is more porous than the B-0 specimen. The platy crystalline $Mg(OH)_2$ may have less of a binding effect than the amorphous CSH, contributing to its relatively lower compressive strength. In contrast, as shown in Fig. 5b, after carbonation curing, many round-shaped crystals were formed in the B-40 mortar. The EDX analysis reveals that the crystals are magnesium calcite, which supports the XRD results shown in Fig. 2. The magnesium calcite forms due to the incorporation of Mg in $CaCO_3$ during the carbonation process [23]. The grain size of a single round magnesium calcite is greater than approximately 0.5 μm and closely agglomerated which may form a stronger microstructure than that of the dispersed $Mg(OH)_2$ crystals in the atmosphere-cured B-40 specimen. Magnesium calcite was also observed in the carbonation cured B-20 specimen.

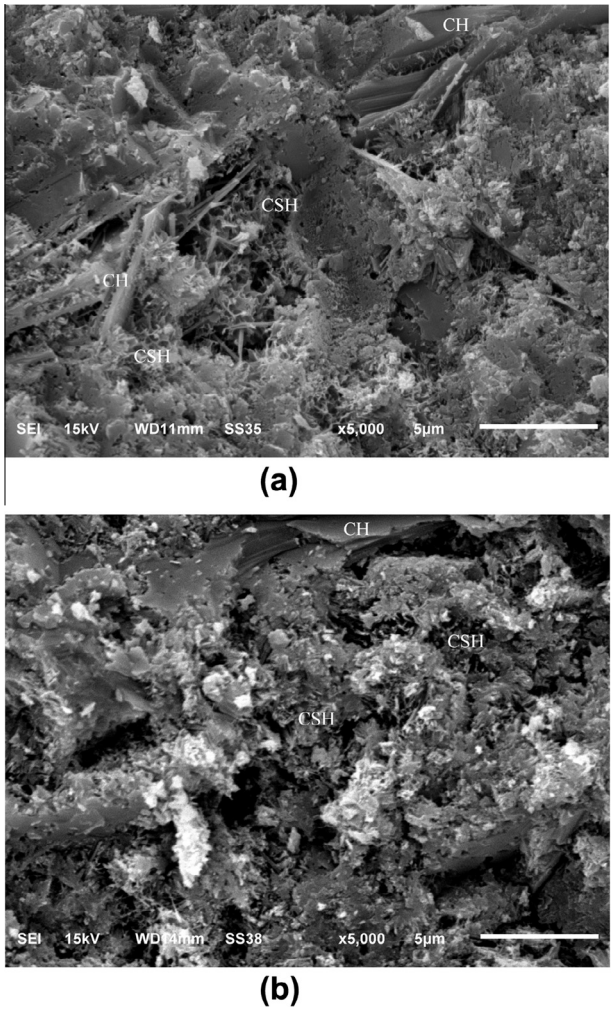

Fig. 4. Typical SEM images of B-0 specimens after 56 d of: (a) atmosphere curing and (b) carbonation curing.

Fig. 6 shows typical SEM images of T-0, T-20 and T-40 specimens after 56 d of carbonation curing. A large amount of cement hydration products remained uncarbonated in the T-0 specimen (Fig. 6a). Fig. 6b of the T-20 mortar reveals the formation of round-faced magnesium calcite aggregates that were interconnected with other phases, which may be $CaCO_3$ or CSH. Some phases likely consisting of pozzolanic reaction products or carbonates were formed around the anhydrous GGBFS particle. In the T-40 mortars, Fig. 6c shows relatively larger agglomerates consisting of magnesium calcite that appear to be quite interconnected.

Fig. 7 shows BSEM images of cement specimens containing reactive MgO after 56 d of carbonation curing. Fig. 7a illustrates magnesium calcite surrounded by Ca-rich phases (likely $CaCO_3$ or CSH), and uncarbonated $Ca(OH)_2$ in the B-20 mortar. Fig. 7b shows a considerable amount of uncarbonated GGBFS surrounded by carbonates and/or uncarbonated CSH in the T-20 mortar specimen. Fig. 7c shows two main features of the T-40 sample, namely the interconnected magnesium calcite phases, and the unhydrated and uncarbonated GGBFS grains. Some carbonates were formed around the GGBFS particle which is probably due to the carbonation of the pozzolanic reaction products of GGBFS. However, as shown in Fig. 7, the carbonation degree of GGBFS in the mortars is relatively low, particularly in T-0 and T-20. The microstructure of the T-40 specimen appears to be more porous, which may be associated with less GU cement used in the specimen.

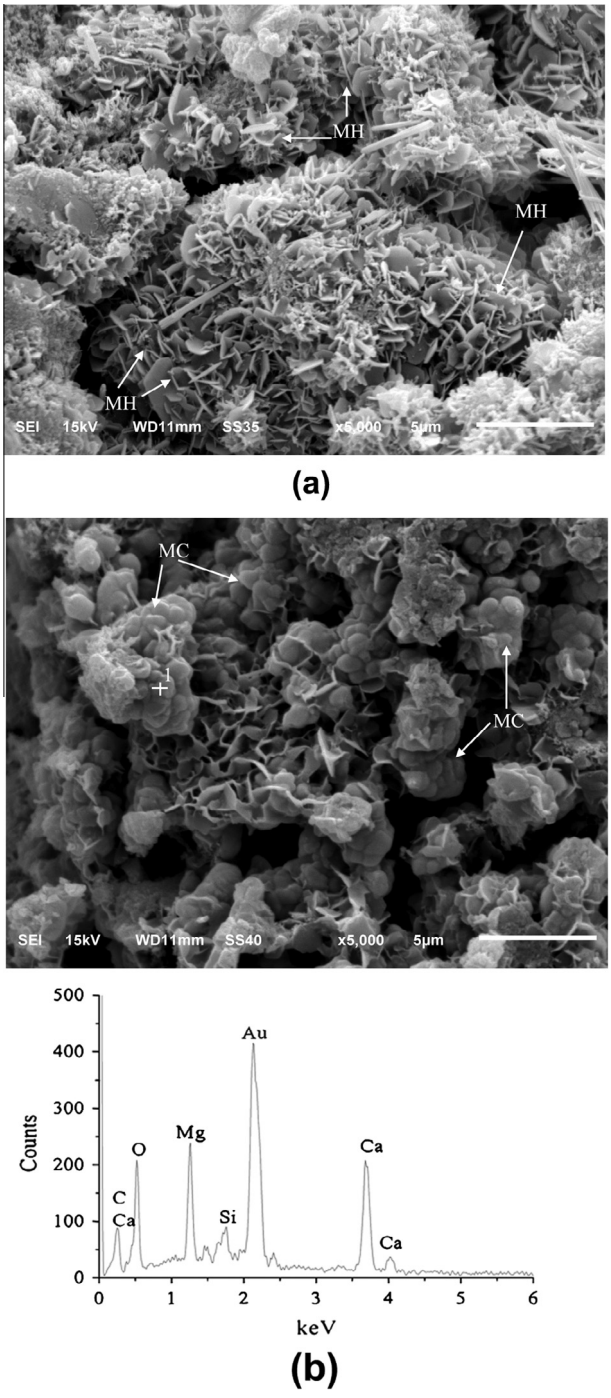

Fig. 5. Typical SEM images of B-40 specimen after 56 d of: (a) atmosphere curing and (b) carbonation curing (CH: portlandite; CSH: calcium silicate hydrate; MC: magnesium calcite; MH: brucite).

3.5. Discussion

3.5.1. Carbonation of GU cement, reactive MgO, and GGBFS mortars

In all mortar mix designs, $Ca(OH)_2$ is the most soluble phase of cement hydration products and is the first to carbonate to form $CaCO_3$. The precipitation mode of $CaCO_3$ during carbonation depends on the diffusion rate of both Ca^{2+} and CO_3^{2-} [28]. If the rate of diffusion of CO_3^{2-} is greater than that of Ca^{2+}, $CaCO_3$ will precipitate on the surface of $Ca(OH)_2$, forming a carbonate layer around $Ca(OH)_2$, which in turn hinders or slows carbonation processes. In contrast, if the rate of diffusion of the Ca^{2+} ions into the pore

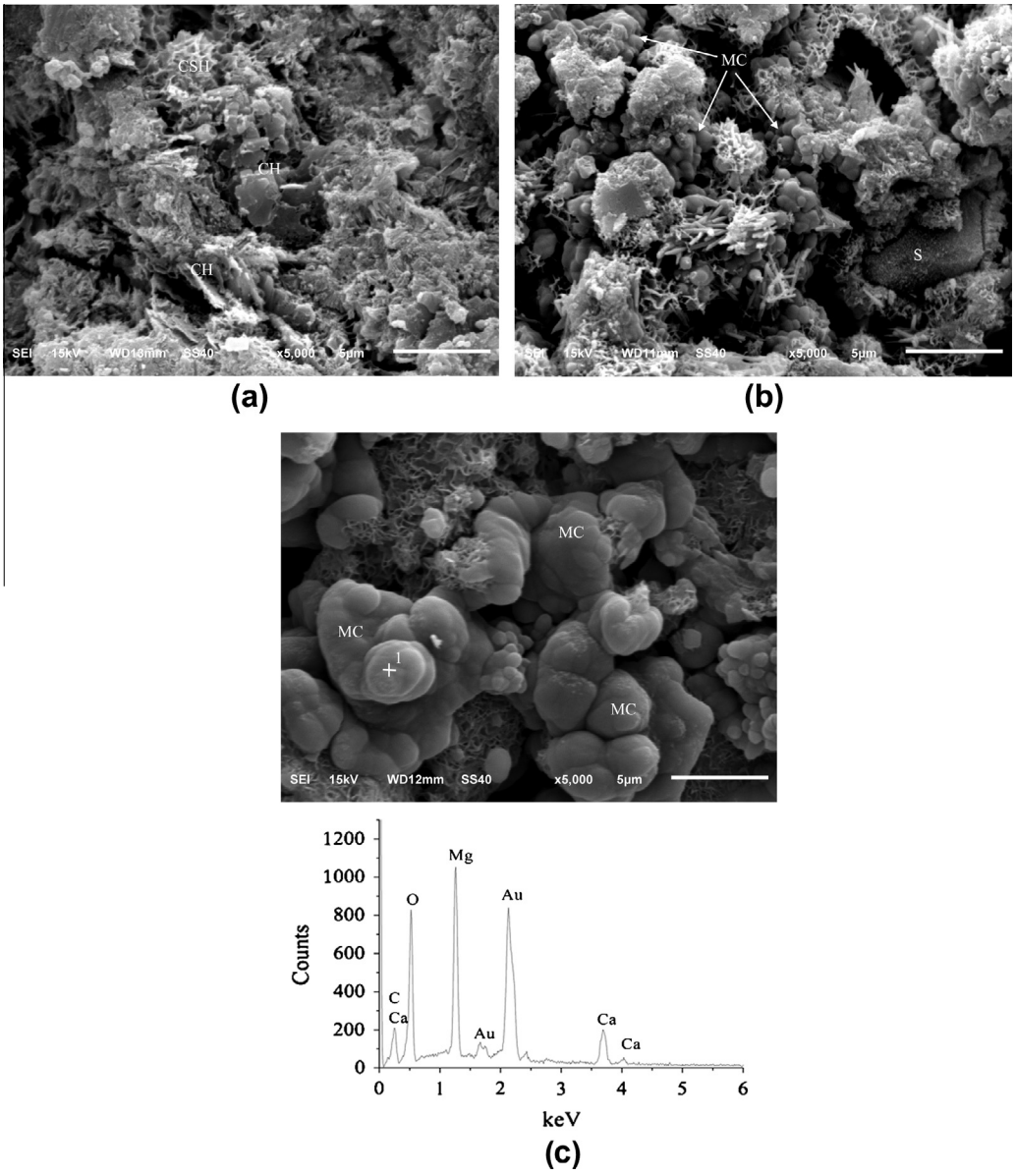

Fig. 6. Typical SEM images of specimens after 56 d of carbonation curing: (a) T-0; (b) T-20; and (c) T-40; and the EDX analysis at point 1 (CH: portlandite; CSH: calcium silicate hydrate; MC: magnesium calcite; S: GGBFS).

solution is faster, $CaCO_3$ is more likely to precipitate in capillary pores [28]. In the accelerated carbonation environment of 99.9% CO_2, the concentration of CO_3^{2-} is relatively high and thus is anticipated to diffuse at a relatively faster rate compared to Ca^{2+}. Accordingly, besides the precipitation of $CaCO_3$ in the pore solution, the CO_3^{2-} may also diffuse to the surface of $Ca(OH)_2$ and precipitate as $CaCO_3$ on the surface of $Ca(OH)_2$, which may inhibit further dissolution of $Ca(OH)_2$ and reduce the rate of carbonation. The precipitation of $CaCO_3$ in pores may also block the pore system and in turn obstruct the further ingress of CO_2.

In contrast to the B-0 mortar specimens, Mg^{2+} coexists with Ca^{2+} in the pore solution of B-20 and B-40 mortars due to the dissolution of $Mg(OH)_2$ and/or reactive MgO. During the carbonation-curing process, Mg^{2+} is incorporated into $CaCO_3$ when the carbonate phase precipitates from the supersaturated solution described in the following equation:

$$Mg^{2+} + Ca^{2+} \rightarrow Ca_xMg_{(1-x)}CO_3 \quad (2)$$

The amount of Mg that can be incorporated in the carbonates depends on the saturation index of $MgCO_3$ in the supersaturated solution [29]. The higher the saturation index, the more Mg can be included in the magnesium calcite phase [29]. $Mg(OH)_2$ has a much lower solubility than $Ca(OH)_2$, which may limit the diffusion of Mg^{2+} and in turn result in a slower carbonation rate [23]. Owing to the relatively slow diffusion of Mg^{2+}, the high magnesium carbonate phase (i.e., high magnesium calcite) is more likely to precipitate close to $Mg(OH)_2$. This is similar to the formation of magnesium calcite in the cement pastes [24]. A recent study by Mo and Panesar [24] revealed that $MgCO_3{\cdot}3H_2O$ formed in cement pastes containing 40% reactive MgO after 56 d of carbonation curing. However, in this study, no $MgCO_3{\cdot}3H_2O$ was identified in any mortar samples. One potential explanation is related to the insufficient supply of CO_3^{2-} due to the blockage of cement hydration products and calcium carbonates formed on the surface of $Mg(OH)_2$. A sufficient supply of CO_3^{2-} is required for the carbonation of $Mg(OH)_2$. This is supported by Fig. 1, which shows that

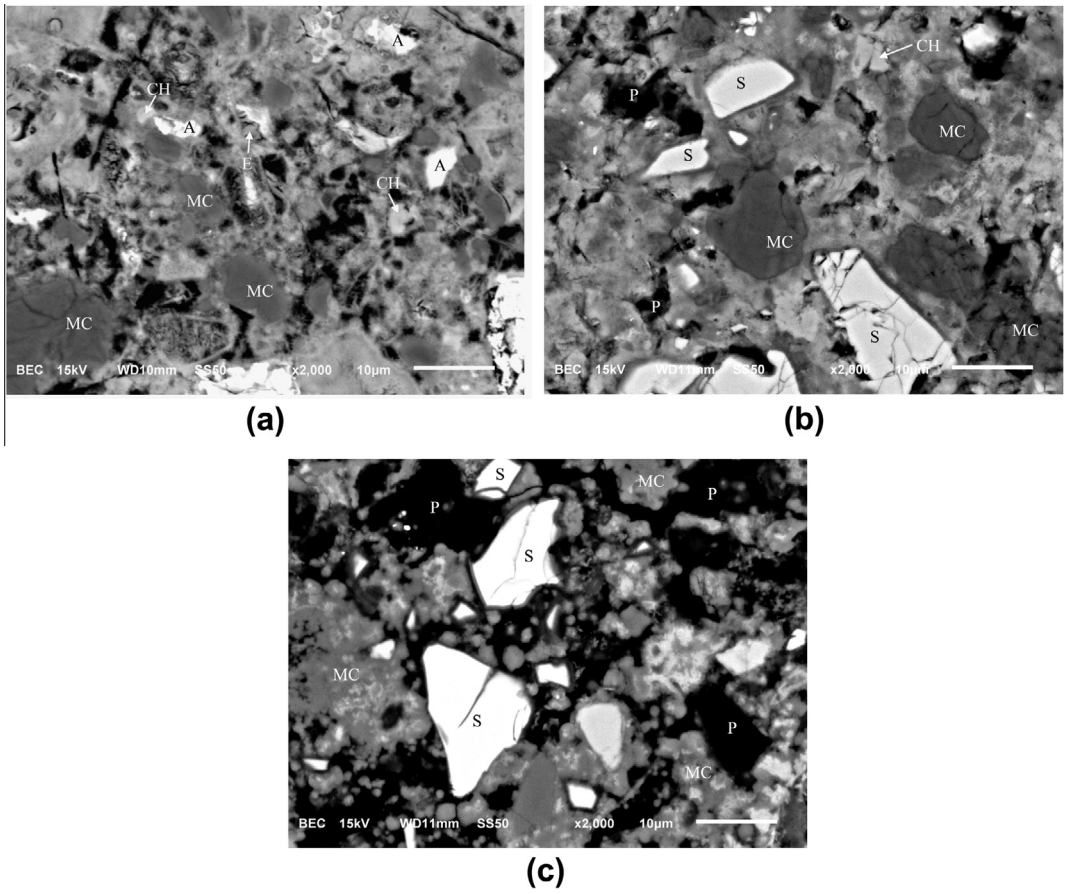

Fig. 7. Typical BSEM images of cement mortar specimens containing reactive MgO after 56 d of carbonation curing: (a) B-20; (b) T-20; and (c) T-40 (CH: portlandite; MC: magnesium calcite; P: pore; S: GGBFS).

not every sample was fully carbonated even after 56 d of exposure, implying that the diffusion of CO_2 or CO_3^{2-} is potentially hindered due to the cement hydration products, carbonate phases and the co-existence of H_2O.

For T-0, T-20 and T-40 mortar specimens, the presence of 40% GGBFS as cement replacement influences the carbonation of cement materials system in three potential ways. Firstly, the pozzolanic reaction of GGBFS consumes some $Ca(OH)_2$ and increases the amount of CSH, which reduces the carbonation rate. Secondly, carbonation of cement-based materials containing GGBFS, particularly with high cement replacement levels ($\geqslant$40%), may coarsen the pore structure, facilitate the diffusion of CO_2 or CO_3^{2-}, and yield a greater rate of carbonation. Thirdly, the GGBFS also participates in the carbonation reaction mainly in terms of the carbonation of its latently hydraulic and pozzolanic reaction products, CSH, which also provides Ca^{2+} necessary for the formation of $CaCO_3$ and/or magnesium calcite. Leaching of Ca^{2+} from GGBFS may be the rate-determining reaction step for GGBFS carbonation [30]. However, the carbonation product layer formed around the GGBFS particles as well as the uncarbonated pozzolanic reaction products may inhibit the further carbonation of anhydrous GGBFS. As a result, the amount of Ca^{2+} and Mg^{2+} leached directly from GGBFS particles may be limited due to the barrier of hydration product rim and the carbonate layers formed around the GGBFS particle as shown in Fig. 7b and c.

Although the moisture in the capillary pore system was removed by the vacuum drying prior to carbonation-curing, as carbonation proceeds, the carbonation of $Ca(OH)_2$ yields H_2O. Furthermore, H_2O may penetrate into the capillary pores as a result of the high relative humidity (98%) condition of the curing chamber. This may block the diffusion of CO_2 and reduce the rate of carbonation. After 56 d of carbonation curing, none of the specimens were fully carbonated as supported by the results in Figs. 1 and 2. In comparison with specimens B-0, B-20 and B-40, specimens T-0, T-20 and T-40, respectively, have a relatively higher degree of carbonation (Fig. 1). This may be related to the relatively more porous microstructure of specimens containing GGBFS and reactive MgO prior to the carbonation curing, and may also be a result of GGBFS carbonation, which encourages CO_2 penetration.

3.5.2. Evolution of microstructure and compressive strength

With atmosphere-curing, the hydration products of GU cement, particularly CSH, is the main binder phase that contributes to the mortar's compressive strength gain. In comparison with CSH, the hydration products of reactive MgO, namely crystalline $Mg(OH)_2$, may have less of an effect on compressive strength development. Increasing the amount of reactive MgO reduces the amount of CSH and increases the amount of $Mg(OH)_2$, which results in the formation of a porous microstructure and a relatively lower compressive strength of specimens as shown in Table 3. There was no evident interplay between the hydration of reactive MgO and Portland cement on compressive strength development based on the results in this study and [31].

The compressive strengths of specimens exposed to carbonation curing increase significantly as the duration of curing increases. This is closely associated with the formation of carbonate phases and correspondingly contributes to the evolution of the microstructure. In addition to the hydration products of GU cement, $CaCO_3$ was formed due to the partially carbonated cement hydration products, which contributed to a denser microstructure

and thus enhanced the development of compressive strength. In the specimens containing reactive MgO, large round-shaped magnesium calcite was formed due to the incorporation of Mg in $CaCO_3$. The incorporation of Mg strongly influenced the morphology of $CaCO_3$ and promoted the aggregation of carbonate phases (Figs. 5–7). This is supported by Meldrum and Hyde [32], who reported that a single magnesium calcite crystal containing up to approximately 10% $MgCO_3$ typically exhibits round faces and edges. The influence of Mg on the morphologies of $CaCO_3$ is influenced by the $CaCO_3$ nucleation and growth process [32]. As reported by de Silva et al. [22], the morphology of $CaCO_3$ is the key factor that controls the compressive strength of carbonate binder, and well-crystallized carbonate results in higher compressive strength. Accordingly, the interconnected microstructure and relatively higher compressive strength of carbonation-cured specimens compared to atmosphere-cured specimens in mortars containing reactive MgO is due to the formation of close intergrowth and aggregated magnesium calcite.

Due to the relatively low carbonation degree of GGBFS in the mortars, the carbonation products of GGBFS may have slight effects on the microstructure evolution and compressive strength directly. However the incorporation of GGBFS has facilitated the carbonation rate of mortars and in turn increased the carbonation degree of other phases i.e. $Ca(OH)_2$, $Mg(OH)_2$, etc. which indirectly contributes to the evolution of microstructure and properties of the mortars. Moreover, the pozzolanic reaction of GGBFS, particularly occurs at the uncarbonated part of the mortars, contributes to the microstructure evolution and compressive strength growth as well.

4. Conclusions

The influence of accelerated carbonation curing on the microstructure and compressive strength of cement mortars containing up to 40% reactive MgO and 40% GGBFS was investigated. The primary conclusions drawn from this research are:

(1) Calcite was the main carbonate formed in carbonation-cured 100%GU cement mortars as a result of carbonation of hydration products. Mortars containing 20% or 40% reactive MgO as cement replacement showed formations of magnesium calcite due to the incorporation of Mg into $CaCO_3$ during the precipitation process.

(2) For the same mix design and the same exposure age, the compressive strengths of carbonation-cured specimens were greater than the atmosphere-cured mortars owing to the formation of carbonate phases. Increasing the percentage of reactive MgO as cement replacement decreased the compressive strength more for the atmosphere-cured mortars than the carbonation-cured mortars

(3) The compressive strength of carbonation-cured mortars is closely related to the morphology and the amount of carbonate phases formed. The presence of Mg in $CaCO_3$ during the precipitation process facilitated the intergrowth of round-shaped magnesium calcite and promoted the agglomeration of carbonates, which resulted in an enhanced microstructure and higher compressive strengths. The ternary blend T-40 mortar (40% GGBFS and 40% reactive MgO as cement replacement) had markedly less available Ca^{2+} for the formation of carbonate phases and cement hydration products resulting in the lowest compressive strength among all the carbonation-cured mortars. Nevertheless, after 56 d of carbonation curing, the compressive strength of the T-40 specimen was 34.9 MPa, which is close to the 37.7 MPa for the atmosphere-cured B-0 (100% GU) mortar specimen.

(4) The carbonation of GGBFS proceeds mainly through the carbonation of its latent hydraulic and pozzolanic reaction products (CSH) which provides Ca^{2+} necessary for the formation of $CaCO_3$ and/or magnesium calcite. The carbonate products of GGBFS do contribute to the evolution of microstructure and compressive strength of mortars but relatively less than the contribution of reactive MgO because of the relatively low carbonation degree of GGBFS. Incorporation of GGBFS facilitates the CO_2 ingress and carbonation processes largely as a result of the formation of a more porous microstructure of the mortar blends containing GGBFS. In addition, the pozzolanic reaction of GGBFS at uncarbonated zone also contributes to microstructure evolution and compressive strength of mortars.

(5) Although, exposure to 99.9% CO_2 and 98% relative humidity was effective in achieving the desirable compressive strength of reactive MgO binders, all the mortars were not fully carbonated by 56 d of carbonation and thus further research is required to investigate a wider range of carbonation-curing conditions as well as identifying the optimal conditions for a rapider carbonation rate and formation of $MgCO_3 \cdot 3H_2O$.

Acknowledgements

The authors acknowledge Ms. Olga Perebatova and Mr. George Kretschmann from the University of Toronto, Canada for their assistance with the experiments. Prof. Deng Min and Mr. Lu Anqun from Nanjing University of Technology, China are appreciated for providing materials. Financial support from the National Science and Engineering Research Council of Canada, China Scholarship Council/The University of Toronto Joint Scholarship, Jiangsu Natural Science Fund (BK2012427), and the research fund of Key Laboratory for Advanced Technology in Environmental Protection of Jiangsu Province (AE201105) are also gratefully acknowledged.

References

[1] IEA and WBCSD (International Energy Agency and World Business Council for Sustainable Development) Cement Technology Roadmap (2009) Carbon emissions reductions up to 2050, 36p. <http://www.wbcsd.org/DocRoot/mka1EKor6mqLVb9w903o/WBCSD-IEA_CementRoadmap.pdf> [accessed 13.09.11].
[2] van den Heede P, de Belie N. Environmental impact and life cycle assessment (LCA) of traditional and 'green' concretes: literature review and theoretical calculations. Cem Concr Compos 2012;34(4):431–42.
[3] Juenger MCG, Winndfeld F, Provis JL, Ideker JH. Advances in alternative cementitious binders. Cem Concr Res 2011;41(12):1232–43.
[4] Gartner EM, Macphee DE. A physico-chemical basis for novel cementitious binders. Cem Concr Res 2011;41(7):736–49.
[5] Schneider M, Romer M, Tschudin M, Bolio H. Sustainable cement production-present and future. Cem Concr Res 2011;41(7):642–50.
[6] Harrison J. Reactive magnesium oxide cements. Australian Patent Office, Philip, Australian Capital Territory, PCT/AU01/00077 [02.08.01].
[7] Liska M, Al-Tabbaa A. Performance of magnesia cements in pressed masonry units with natural aggregates: production parameters optimisation. Constr Build Mater 2008;22(8):1789–97.
[8] Jerga J. Physico-mechanical properties of carbonated concrete. Constr Build Mater 2004;18(9):645–52.
[9] Shi C, Wu Y. CO_2 curing of concrete blocks. Concr Int 2009(February):39–43.
[10] Sisomphon K, Lutz F. Carbonation rates of concretes containing high volume of pozzolanic Materials. Cem Concr Res 2007;37(12):1647–53.
[11] Sulapha P, Wong SF, Wee TH, Swaddiwudhipong S. Carbonation of concrete containing mineral admixtures. J Mater Civ Eng 2003;15(2):134–43.
[12] de Ceukelaire L, van Nieuwenburg D. Accelerated carbonation of a blast-furnace cement concrete. Cem Concr Res 1993;23(2):442–52.
[13] Sisomphon K, Franke L. Carbonation rates of concretes containing high volume of pozzolanic materials. Cem Concr Res 2007;37(12):1647–53.
[14] Stark J, Ludwig H-M. Freeze-deicing salt scaling resistance of concretes containing blast-furnace slag-cement. In: Marchand J, Pigeon M, Setzer M, editors. Freeze–thaw durability of concrete. London: E&FN Spon; 1997. p. 107–20.

[15] Liska M, Al-Tabbaa A. Ultra-green construction: reactive magnesia masonry products. Proc Inst Civil Eng – Waste Res Manage 2009;162(4):185–96.
[16] Liska M, Vandeperre LJ, Al-Tabbaa A. Influence of carbonation on the properties of reactive magnesia cement-based pressed masonry units. Adv Cem Res 2008;20(2):53–64.
[17] Vandeperre LJ, Al-Tabbaa A. Accelerated carbonation of reactive MgO cements. Adv Cem Res 2007;19(2):67–79.
[18] Xiong Y, Lord AS. Experimental investigations of the reaction path in the MgO–CO_2–H_2O system in solutions with various ionic strengths, and their applications to nuclear waste isolation. Appl Geochem 2008;23(6):1634–59.
[19] Hächen M, Prigiobbe V, Baciocchi R, Mazzotti M. Precipitation in the Mg-carbonate system—effects of temperature and CO_2 pressure. Chem Eng Sci 2008;63(4):1012–28.
[20] Shao Y, Lin X. Early-age carbonation curing of concrete using recovered CO_2. Concr Int 2011(September):50–6.
[21] Rostami V, Shao Y, Boyd AJ, He Z. Microstructure of cement paste subject to early carbonation curing. Cem Concr Res 2012;42(1):186–93.
[22] de Silva P, Bucea L, Moorehead DR, Sirivivatnanon V. Carbonates binders: reaction kinetics, strength and microstructure. Cem Concr Compos 2006;28(7):613–20.
[23] de Silva P, Bucea L, Sirivivatnanon V. Chemical, microstructural and strength development of calcium and magnesium carbonate binders. Cem Concr Res 2009;39(5):460–5.
[24] Mo L, Panesar DK. Effects of accelerated carbonation on the microstructure of Portland cement pastes containing reactive MgO. Cem Concr Res 2012;42(6):769–77.
[25] ASTM C109/C 109M-07. Standard test method for compressive strength of hydraulic cement mortars; 2007.
[26] Venhuis MA, Reardon EJ. Vacuum method for carbonation of cementitious wasteforms. Environ Sci Technol 2001;35(20):4120–5.
[27] Chang CF, Chen JW. The experimental investigation of concrete carbonation depth. Cem Concr Res 2006;36(9):1760–7.
[28] Lagerblad B. CO_2 uptake during the concrete life cycle: carbon dioxide uptake during concrete life cycle – state of the art. Stockholm: Swedish Cement and Concrete Research Institute, CBI; 2006.
[29] Pokrovsky OS. Precipitation of calcium and magnesium carbonates from homogeneous supersaturated solutions. J Cryst Growth 1998;186(1–2):233–9.
[30] Huijgen WJJ, Witkamp GJ, Comans RNJ. Mineral CO_2 sequestration by steel slag carbonation. Environ Sci Technol 2005;39(24):9676–82.
[31] Vandeperre LJ, Liska M, Al-Tabbaa A. Microstructures of reactive magnesia cement blends. Cem Concr Compos 2008;30(8):706–14.
[32] Meldrum FC, Hyde ST. Morphological influence of magnesium and organic additives on the precipitation of calcite. J Cryst Growth 2001;231(4):544–58.